DØ Note 4988
Version 1.34

Evidence for $Z \rightarrow b\bar{b}$ Decays at DØ

Amber Jenkins, Per Jonsson, Gavin Davies
Imperial College London, UK
Andrew Haas
Columbia University, USA

March 13, 2006

Abstract

A search has been performed at DØ for $Z \rightarrow b\bar{b}$ decays using the initial 300 pb^{-1} of data from Run II. Candidate events are selected by triggering on muons from semileptonic decay of b quarks. Trigger and offline b-tagging requirements remove background from light quarks. The remaining $b\bar{b}$ background is harder to suppress. For this purpose, the three most valuable handles are the number of jets per event, the dijet angular distribution and invariant mass. The $b\bar{b}$ background is estimated using b-tag rate functions (TRFs) derived from data. In this analysis on b production two somewhat different background-subtraction methods are explored. Both approaches lead to an an excess of events following background subtraction. One method yields an excess of 1353 $\pm$ 151 (stat.) $\pm$ 306 (syst.) events in 297.5 pb^{-1} of data collected with triggerlist versions 8-12. This excess is in good agreement with Monte Carlo predictions, and amounts to a $Z \rightarrow b\bar{b}$ signal of 4.0 standard deviations. The second approach, which deals with the entire pre-v13 pass1 data, reveals an excess of 810 $\pm$ 230 (stat.) events.

1 Motivation

The measurement of $Z \rightarrow b\bar{b}$ is an important part of the program at DØin that it can provide an independent calibration and efficiency for tagging b quarks. In Run I, the DØ detector lacked a magnetic field, and its tracking capabilities were not as refined; as such the potential for observing $Z \rightarrow b\bar{b}$ was limited. With an upgraded tracking system, improved muon triggering and the possibility of online b-quark tagging the prospects for observing $Z \rightarrow b\bar{b}$ in Run II are brighter. This paper describes the first search for $Z \rightarrow b\bar{b}$ at DØ in Run II of the Tevatron collider.

$Z \rightarrow b\bar{b}$ is a particularly important tool in the calibration of the b-jet energy scale, which affects many analyses of the high-p_T physics at the Tevatron. The current uncertainty on the jet energy scale - of the order of 3% - dominates the uncertainty on the mass of the top quark, and an improved measurement of the b-jet energy scale can further constrain its mass. In addition, $Z \rightarrow b\bar{b}$ can be used to improve the understanding of jet energy resolution.

Another major impetus behind the search is that $Z \to b\bar{b}$ serves as an important benchmark for Higgs physics, since it is the closest observable process to the decay of a light Higgs to $b\bar{b}$. The knowledge of jet energy resolution, dijet mass resolution, b tagging and kinematic handles gleaned in studying $Z \to b\bar{b}$ can be used to refine Higgs searches at a hadron-hadron collider.

The main challenge is to sufficiently reduce backgrounds such that $b\bar{b}$ events from the Z can be observed. To this end, careful analysis techniques are critical and only the most effective triggers must be employed.

2 Event Samples

2.1 The Data

Our analysis uses data collected with several trigger lists, the latest of which is v12. For the v13 list, channel-specific triggers were put in place for the $Z \to b\bar{b}$ search. However, the v13 data suffer from poor statistics, as correspond to an integrated luminosity of only about 50.0 pb^{-1}. More events are needed both to ensure statistical significance in the search and to model the background with sufficient precision. The analysis is therefore extended to incorporate pre-v13 data, corresponding to an integrated luminosity of approximately 300 pb^{-1}. In fact, the analysis described in the following will concentrate largely on the pre-v13 sample. See Appendix A for more information on the v13 triggers and data.

The data arise from the "BID" skim, processed and fixed with the pass2 p14 version of the reconstruction software.[1] The skim has the following properties:

- A "loose" offline reconstructed muon in each event, with $p_T > 4$ GeV/c, matched within ΔR <0.7 to a jet of cone radius 0.5. (A cone radius is specified by $\Delta R = \sqrt{(\Delta\phi)^2 + (\Delta\eta)^2}$, with ϕ and η being the azimuth and pseudorapidity.) This requirement enhances the fraction of heavy-flavour events due to the decays of $b \to \mu$ and $b \to c \to \mu$;[2]
- The skim contains about 90 million events, and corresponds to integrated luminosities of about 50 pb^{-1} and 300 pb^{-1} for the v13 and pre-v13 data, respectively.

The following selection criteria are imposed to ensure good data quality:

- Events are required to be contained in acceptable luminosity blocks.
- Good calorimeter and jet/Missing E_T response in runs.
- Runs with acceptable muons.
- Runs with acceptable central-tracking information (SMT and CFT).

2.2 Monte Carlo

A range of Monte Carlo (MC) samples are used in the analysis as listed in Table 1. Each MC sample is generated with Pythia, overlaid with an average of 0.8 minimum bias events, passed through a full GEANT simulation of the detector, and processed with version p14 of the reconstruction software.

[1] The analysis in Section 7 uses the pass1 p14 data

[2] The BID skim provided the best data available at the time of this analysis. A new skim, "2JET", has been proposed for future use, which would require exactly two 0.5 cone jets, each with $p_T > 15$ GeV/c, but not demand any muons. Initial studies indicate that the total efficiency for signal would increase by 50–100% using this skim.

Monte Carlo Sample	p_T Cut Applied at Parton Level, GeV/c	Number of Events
	Signal	
$Z \to b\bar{b}$	None	82,000
	Heavy-flavour Backgrounds	
$b\bar{b}$	5–20	200,000
$b\bar{b}$	20–40	125,000
$b\bar{b}$	40–80	150,000
$b\bar{b}$	80–160	100,000
$b\bar{b}$	160–320	25,000
$b\bar{b}$	> 40	200,000
	Light-quark (u,d,s) Backgrounds	
$q\bar{q}$	5–20	200,000
$q\bar{q}$	20–40	125,000
$q\bar{q}$	40–80	150,000
$q\bar{q}$	80–160	100,000
$q\bar{q}$	160–320	25,000

Table 1: Summary of Monte Carlo samples used in this analysis. q refers to the light quarks u, d or s.

The data skim and MC samples are processed using either the RASTA or, in Section 7, the higgs_multijet roottuple-generating packages. Jet energy scale corrections are applied to all jets, including corrections for muons in jets, using version 5.3 of the jet energy correction software.[3] No specific b-jet energy scale corrections are applied, as no officially approved corrections exist for these data.

Monte Carlo events are corrected throughout the analysis to account for the b-tagging efficiency and jet measurement effects observed in data. Jet energies are smeared to reflect the jet energy resolution measured in data, and event weighting is applied in order to account for the fact that jet reconstruction/identification and b-tagging are not 100% efficient.

[3]The analysis in Section 7 used an earlier version of the jet energy scale corrections compatible with data from the p14 pass1.

3 Triggers

$Z \rightarrow b\bar{b}$ events are characterised by the presence of two b-tagged jets. Light quark rejection is needed at the trigger level, prior to any offline event selection, in order to achieve an acceptable trigger rate at instantaneous luminosities in excess of 50 x $10^{30}\mathrm{cm}^{-2}\mathrm{s}^{-1}$. Without this rejection, the data would have to be prescaled and candidate events thrown away.

Ideally, the trigger should rely on dijet events with displaced vertices at Level 2, but this capability was provided only recently by the Level 2 Silicon Track Trigger (STT). Alternatively, candidate events can be selected at the trigger level using the semileptonic decay of the b-quarks. However, triggering on muons within one or both b jets from the Z, limits the signal efficiency because of the small $b \rightarrow \mu$ branching fraction.[4] The v8 to v12 trigger lists ran online from 2001 to June 2004; they contain more than 60 different muon-based triggers of interest to this analysis, which were exposed to a luminosity of about 300 pb^{-1}.

The leading muon triggers of the full data sample were identified (i.e. those which were fired most often in data for candidate events after final event selection) and the most significant trigger in the v12 data was selected for the analysis[5].

The most significant v12 and v11 triggers are described in Tables 2 and 3, respectively.

v12 Trigger	**Trigger Description**		
	Level 1	**Level 2**	**Level 3**
MU_JT25_L2M0	single μ + jet	$\geq 1\mu + \geq 1$ jet	≥ 1 jet
MU_2TRK3_L2M0	single μ + jet	$\geq 1\mu$	2 global tracks
MUW_W_L2M3_TRK10	single μ	$\geq 1\mu$	1 global track

Table 2: Description of the three leading v12 muon triggers. Candidate signal events were required to pass MU_JT25_L2M0.

v11 Trigger	**Trigger Description**		
	Level 1	**Level 2**	**Level 3**
MU_JT20_L2M0	single μ + jet	$\geq 1\mu + \geq 1$ jet	≥ 1 jet
MU_JT25_L2M0	single μ + jet	$\geq 1\mu + \geq 1$ jet	≥ 1 jet
MUW_W_L2M3_TRK10	single μ	$\geq 1\mu$	1 global track

Table 3: Description of the three leading v11 muon triggers. Candidate signal events were required to pass MU_JT25_L2M0.

Trigger efficiencies for the v12 and v11 triggers are listed in Tables 4 and 5.

[4] B.R.(b $\rightarrow \mu$) = 0.11. Muons from the cascade decays $b \rightarrow c \rightarrow \mu$ and $b \rightarrow \tau \rightarrow \mu$ are significant, and the total probability for a b-jet to have a muon is nearly 20%. For $Z \rightarrow b\bar{b}$ events in which *at least one* b-jet has a muon which passes muon cuts, the maximum signal efficiency hence is $1 - (1 - 0.2)$x$(1 - 0.2) = 36\%$. For events with two muons, this number reduces to 4%.

[5] This trigger selection does however not apply to the analysis presented in Section 7, which treats the entire data as a whole

v12 Trigger	**L1L2L3 Trigger Efficiency(%)**	
	Absolute	**w.r.t. Offline Cuts**
MU_JT25_L2M0	5.5	15.6
MU_2TRK3_L2M0	7.0	18.1
MUW_W_L2M3_TRK10	3.4	8.9
OR of the above 3 triggers	8.7	20.2

Table 4: v12 trigger efficiencies for MC signal events.

v11 Trigger	**L1L2L3 Trigger Efficiency(%)**	
	Absolute	**w.r.t. Offline Cuts**
MU_JT20_L2M0	7.4	18.3
MU_JT25_L2M0	5.5	15.6
MUW_W_L2M3_TRK10	3.4	8.9
OR of the above 3 triggers	8.4	19.7

Table 5: v11 trigger efficiencies for MC signal events.

The most frequently fired v12 trigger, MU_JT25_L2M0, was exposed to a luminosity of 297.5 pb^{-1}. To simplify the analysis and the comparison to the MC predictions all events in the pre-v13 data were selected from this single trigger.[6]

[6] As previously noted, the analysis presented in Section 7 does not apply this trigger selection.

4 Event Selection

There are few kinematic handles with which to discriminate between the $Z \rightarrow b\bar{b}$ signal and the QCD $b\bar{b}$ background. The two most powerful variables, besides the invariant di-jet mass, are the number of jets in the event, n_{jet} and the angular separation of the two leading b-jets, $\Delta\varphi$. Intuitively, for a given jet p_T, one would expect the two leading jets to be more back-to-back in $Z \rightarrow b\bar{b}$ events than in QCD background, due to the color connection between initial and final state and hence the presence of more gluon radiation in the QCD processes.

With this in mind, candidate events are selected using the following offline prescription:

Cut 1 Trigger selection: MU_JT25_L2M0;

Cut 2 The event must contain two and only two good quality jets and at least one loose offline muon;

Cut 3 The two jets must both have $|\eta| < 2.5$ and corrected $p_T > 15$ GeV/c;

Cut 4 For b-tagging, the two jets must both be taggable;

Cut 5 The primary vertex of the event must have more than 2 tracks attached to it and be located within ± 50 cm in the z-direction;

Cut 6 The two jets must both be "loose" SVT-tagged (using the standard p14 definitions);

Cut 7 The two b-jets must be strongly back-to-back, i.e. $\Delta\varphi > 2.75$ radians.

Tables 6 and 7 show the number of events passing each analysis cut in signal MC and data. Monte Carlo event counts are weighted by cross-section and luminosity.

Analysis Cut	**Number of Events Passing Cut, pre-v13**
No selection	336475 ± 1174
1	18567 ± 276
2	10524 ± 209
3	8055 ± 183
4	6915 ± 169
5	6643 ± 165
6	1451 ± 77
7	1444 ± 65

Table 6: Cut flow table for $Z \rightarrow b\bar{b}$ Monte Carlo events passing pre-v13 triggers. Event counts are weighted by cross-section and luminosity, the errors are statistical only.

In the BID skim the bb/light quark fraction is about 10% after a single b-tag requirement (see Fig. 16). With the additional muon and trigger selection (Cuts 1 and 2) the bb/light fraction is about 20% and after requiring a double offline b-tag in the data (Cut 6) the light-quark QCD background component is reduced to about 10% of the sample. However, a large heavy-flavour component remains which still swamps the signal; S:(S+B) is of the order of 1:20. By restricting the number of jets and the angle between the two b-jets (i.e. cuts 2 and 7) the signal significance can

Analysis Cut	**Number of Events Passing Cut, pre-v13**
1	10882864
2	5135730
3	4030914
4	2726889
5	2698544
6	33499
7	31183

Table 7: Cut flow table for events in data. Note the much higher fraction of events passing the offline criteria in the v13 data.

be improved. We have investigated the effect of these two cuts on the effective signal significance, where effective significance is defined as

$$\textit{Effective Significance} = \frac{N_{signal}}{\sigma^{stat}_{bkg} \oplus \sigma^{syst}_{bkg} \oplus \sqrt{N_{tot}}} \tag{1}$$

Here N_{signal} is the number of MC signal events passing the cuts, weighted by cross-section and luminosity, σ^{stat}_{bkg} and σ^{syst}_{bkg} are the statistical and systematic errors on the estimated number of background events passing all cuts and N_{tot} is the total number of events in data passing the cuts. In what follows, the square root of N_{tot} - N_{signal} is used as a conservative estimate of the size of the statistical error on the background; see Section 6 for how this error is calculated in the actual analysis.

Figure 1 shows the variation of effective signal significance with the cut on the number of jets in the event and indicates that restricting the number of jets to exactly two provides the best significance. Requiring two and only two jets desirably cleans up the signal by restricting the amount of radiation between the jets.

In Figure 2 we compare the azimuthal angle between the two jets for signal and data, after applying cuts 1–6 and accounting for the trigger efficiency and the integrated luminosity of 297.5 pb^{-1}. The signal:background ratio is 1:23 and, as expected, the jets in $Z \to b\bar{b}$ are slightly more back-to-back than in the background. Effective significance is plotted as a function of $\Delta\varphi$ cut in Figure 3, while varying the systematic part of the error on the background. Taking into account the triggger efficiency and integrated luminosity, a significance of 4 is obtained with a cut of $\Delta\varphi > 2.75$ radians and a background systematic uncertainty of 1% (see Section 6 for a discussion of background uncertainties.). Note that so far no invariant mass cut has been applied. Since the signal events are expected to be concentrated in an invariant mass window around the Z mass(see Figure 4), such a cut around the interesting region can be expected to further enhance the significance of the signal. We can therefore conclude that an excess of $Z \to b\bar{b}$ events of the order of 4 sigma above the background may already be observable in the pre-v13 data sample, if the background can be estimated with sufficient precision.

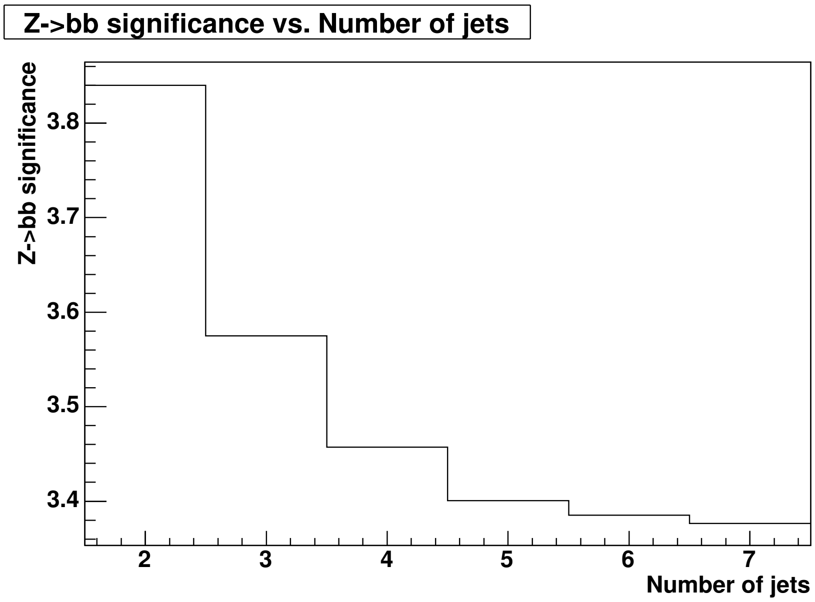

Figure 1: Effective signal significance, before cut 7, as a function of the cut on the number of good jets in the event, n_{jet}, in the pre-v13 data. The systematic error on the number of background events was set to 1%. Maximum significance is obtained in events with two and only two jets.

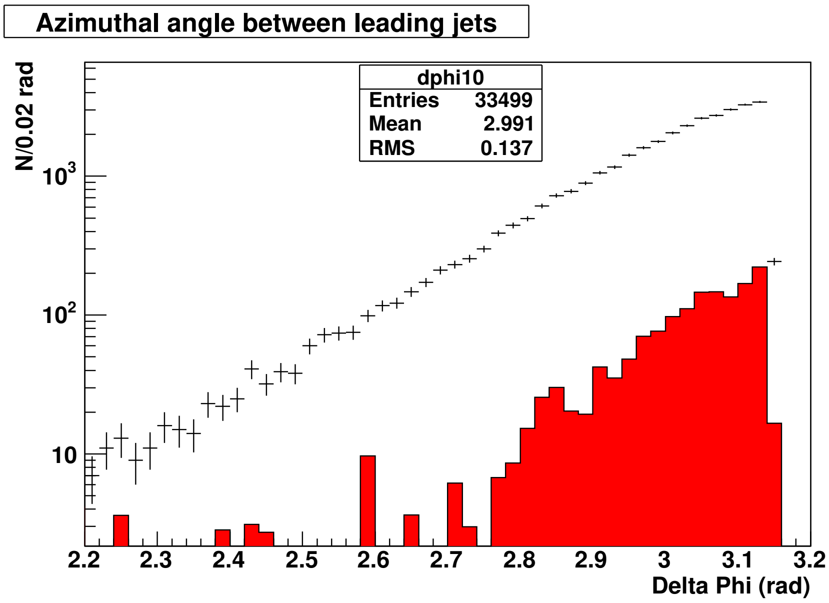

Figure 2: Comparison of the angular dijet distribution between pre-v13 data and signal MC, after passing cuts 1–6. Red (dark grey) histogram: MC signal; black points: data. The signal is slightly more back-to-back and S:S+B is approximately 1:23.

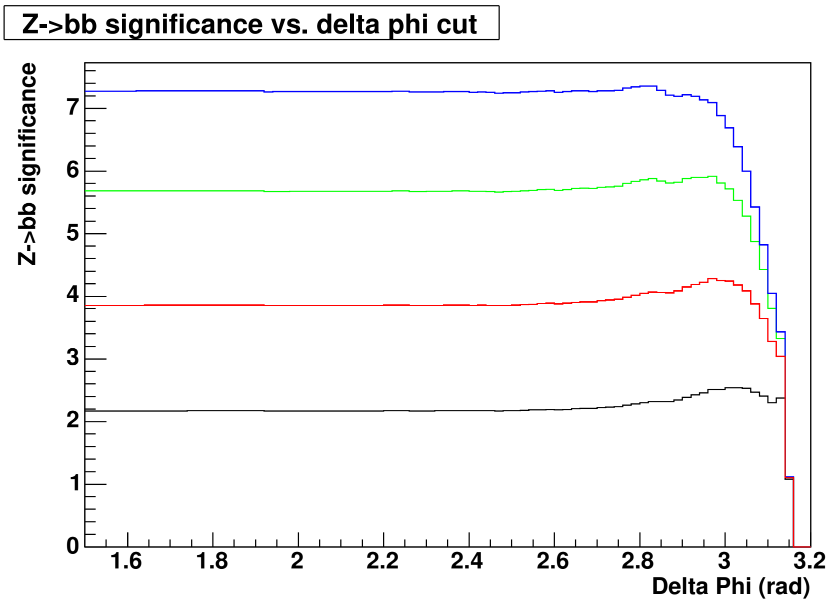

Figure 3: Effective signal significance as a function of $\Delta\varphi$ cut in pre-v13 data, for a systematic error of (from top to bottom) 0% (blue), 0.5% (green), 1% (red), and 2% (black) on the number of background events. The dependence on $\Delta\varphi$ is weak and a loose cut of 2.75 was used in the pre-v13 analysis.

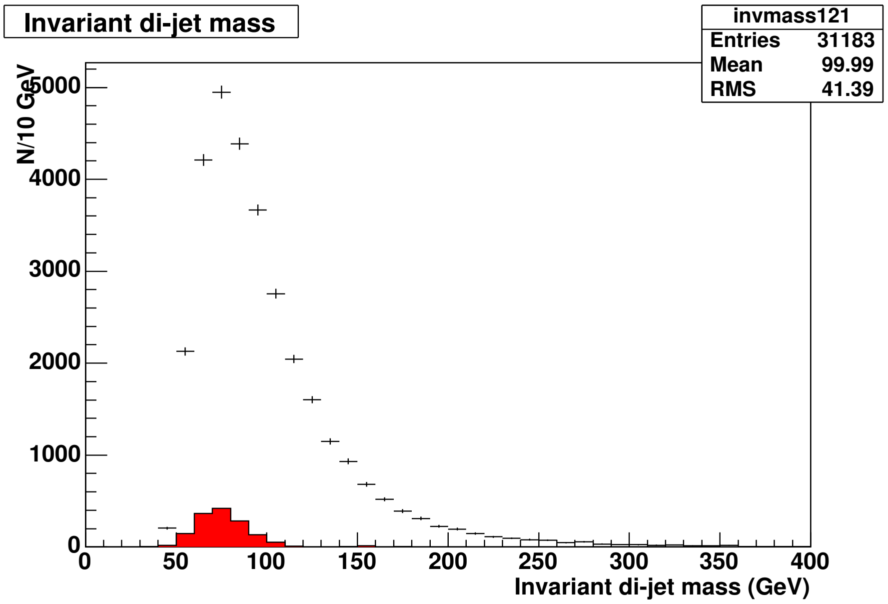

Figure 4: Comparison of the invariant dijet mass after event selection in pre-v13 data (black) and the expected $Z \rightarrow b\bar{b}$ MC signal (red). No b-jet energy scale correction is available for this data, which explains why the Z mass peak is shifted towards lower masses. Note that the region above 120 GeV is almost signal free.

5 Background Subtraction

Understanding the background to the $Z \to b\bar{b}$ signal in the double b-tagged data sample is as we have seen crucial to this analysis. The background is composed almost entirely of heavy-flavour dijet production and mistagged gluon/light-quark jet production, all of which cannot be accurately simulated using current techniques. Thus the background is derived from data, using either single-tagged and/or untagged events. Once the background shape is well understood, one can then subtract it from the data with confidence.

We have developed two slightly different methods for measuring the background. The two approaches have different strengths and weaknesses and are discussed in Sections 6 and 7 respectively. Both methods use a *tag rate function (TRF)* to estimate the amount of double b-tagged background in the data. We measure the *tag ratio* of double to single b-tags as a function of jet p_T and jet η to form the TRF.

The first method (Section 6) defines signal and background 'zones' in terms of $\Delta\varphi$. A TRF is constructed using information from the signal zone and then applied, as an event weight, to the single tagged events in the same signal zone. The final invariant mass background template is then normalized to the double tagged data with a fit to the signal free invariant mass region above 120 GeV. As a comparison, the result of using the TRF from a background zone with $\Delta\varphi < 3.0$ can be found in Appendix B.

The second approach (Section 7) does not prescribe signal and background regions and instead uses a single data sample. In addition, two corrections are applied to account for differences between single b-tagged and untagged events and also to incorporate signal events which are not double b-tagged.

6 Background Estimation Method 1

6.1 Background Estimation Using an Invariant Mass Based TRF

A convenient starting point to this analysis is the strategy and method used by the CDF $Z \to b\bar{b}$ analysis in Run I [1].

One can attempt to estimate the background by defining two regions in $\Delta\varphi$ space:

1. *"In Zone":* A region rich in signal. Events falling into this box pass Cuts 1–5 and Cut 7 (as outlined in Section 4). Cut 7, the cut of $\Delta\varphi > 2.75$ radians, ensures a more back-to-back like topology in the event.

2. *"Out of Zone":* A background-enriched region. Events only pass Cuts 1–5. They fail Cut 7, the 'in zone' $\Delta\varphi$ criterion.

The data are then further divided into a double-b-tagged sample (by imposing Cut 6) and a single-b-tagged sample. There are thus four types of events:

- In Zone, double-tagged: N_{in}^{++}
- In Zone, single-tagged: N_{in}^{+}
- Out of Zone, double-tagged: N_{out}^{++}
- Out of Zone, single-tagged: N_{out}^{+}

In the signal-enhanced region, N_{in}^{++} is an admixture of genuine signal events plus background events. The amount of background in-zone can be naively determined by calculating the tag-ratio of double to single b-tags outside the zone and then applying this TRF into the zone. Here the TRF is defined as the ratio between N_{out}^{++} and N_{out}^{+}. An estimate of the expected background in-zone is then for each invariant mass bin given by

$$(N_{in}^{++})_{exp}^{bkg} = (N_{in}^{+})_{obs} \text{ x } \frac{(N_{out}^{++})_{obs}}{(N_{out}^{+})_{obs}}. \tag{2}$$

$(N_{in}^{++})_{exp}^{bkg}$ can then be subtracted bin-by-bin from the invariant mass spectrum obtained after applying Cuts 1–7. After subtraction, provided the number of events occupying the side-band regions is consistent with zero, an excess around the mass of the Z constitutes evidence for a signal.

Underpinning this method is the assumption that it is valid to extrapolate a TRF measured *outside* the signal zone *into* the signal zone. This in turn assumes that the TRF is independent of the choice of signal box, in particular of the choice of $\Delta\varphi$ between the two leading jets in the event, and is discussed further in Section 6.2. In addition, signal events that appear out-of-zone are neglected, resulting in a somewhat conservative signal estimate. In reality, a small amount of $Z \to b\bar{b}$ will also be present outside the zone (see Figure 2).

6.2 Correction for the $\Delta\varphi$ Dependence of the TRF

Up to this point, it has been assumed that the ratio of double- to single-tags outside the signal zone is independent of where the signal box is placed, i.e. is independent of the particular $\Delta\varphi$ value chosen to differentiate signal from background. Figure 5 which shows the double to single tag rate as a function of $\Delta\varphi$, however suggests a strong linear dependence.

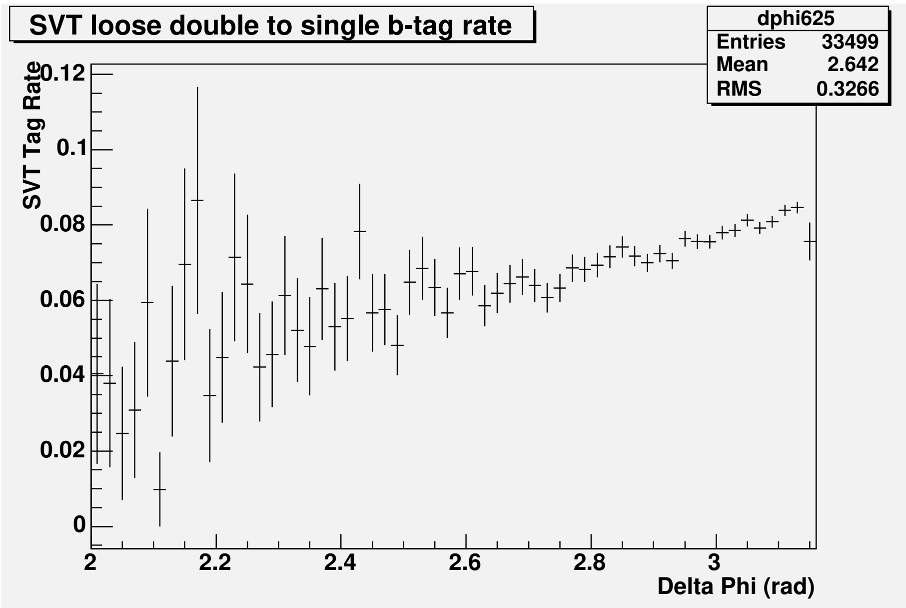

Figure 5: The variation of tag-rate function with $\Delta\varphi$ between the two leading b-jets in each event, for pre-v13 data. A linear dependence of the TRF upon $\Delta\varphi$ is observed.

A similar dependence of the TRF is also observed in Monte Carlo.

Having demonstrated that a clear $\Delta\varphi$ dependence exists, it is natural to evaluate and apply a correction for this dependence. Our initial approach involved deriving the correction by fitting a plot of the tag ratio against $\Delta\varphi$ from data outside the signal zone. As $\Delta\varphi$ increases, the ratio of double- to single-tags increases linearly. This linear dependence can be fitted and extrapolated from the mean value of $\Delta\varphi$ outside the zone to the average $\Delta\varphi$ value inside the zone. This method, however, results in a rather large systematic uncertainty on the number of background events.
A more accurate method to take the $\Delta\varphi$ dependence into account is instead to normalize the TRF weighted invariant mass distribution to the double-tagged data by fitting it to the observed signal depleted region above 120 GeV. A possible weakness of this method is that it does not account for any $\Delta\varphi$ dependent invariant mass bias. Another approach, which will remove any such $\Delta\varphi$ dependent difference between the events used for the TRF and the selected in-zone events and also result in larger statistics for the background determination, is to calculate the TRF from the same in-zone events to which it will be applied and then again fix the overall normalisation by fitting the invariant mass distribution to the data above 120 GeV. In the following we will use this method to model the background.

The main challenge arising from this method is the difficulty of obtaining a sufficiently precise normalisation fit of the invariant mass to the double tagged data. The systematic uncertainty of the background which, as we have seen, is critcal to extract a signal of any significance, is dominated by the error on this fit.

6.3 Improving the TRF Further: The Jet-Based TRF Method

In addition to correcting for the $\Delta\varphi$ dependency of the TRF, we can improve the way in which the TRF is calculated. Instead of an invariant-mass based TRF, a TRF can be constructed on a jet-by-jet basis. This is a similar approach to that adopted in the DØ Run II $hb\bar{b}$ analysis [2].

This approach can still be based on either events inside or outside the signal zone. Consider events in which the first-leading jet is single-SVT loose tagged. For these events, the second leading jet is categorised according to its location in one of three different eta regions of the detector: $|\eta| < 1.1$, $1.1 < |\eta| < 1.5$ and $1.5 < |\eta| < 2.5$. For each η region, the TRF is then parametrised as a function of the p_T of the second leading jet. This generates a TRF *per jet*.

To estimate the background in-zone, each event passing Cuts 1–5 and 7 and with the leading jet loose SVT b-tagged is weighted by the TRF corresponding to the second leading jet. This is likely to be a more accurate method as it provides a finer resolution to the correction. The resulting background distribution is then corrected for the dependence of the TRF upon $\Delta\varphi$ by fitting it to the observed invariant mass distribution above 120 GeV (as discussed in Section 6.2). Figure 6 illustrate the jet-based TRF as a function of the second leading jet p_T, for jets in three different η-bins: $|\eta| < 1.1$, $1.1 < |\eta| < 1.5$, and $1.5 < |\eta| < 2.5$ for in-zone events (See Appendix B for the TRF from the out-zone).

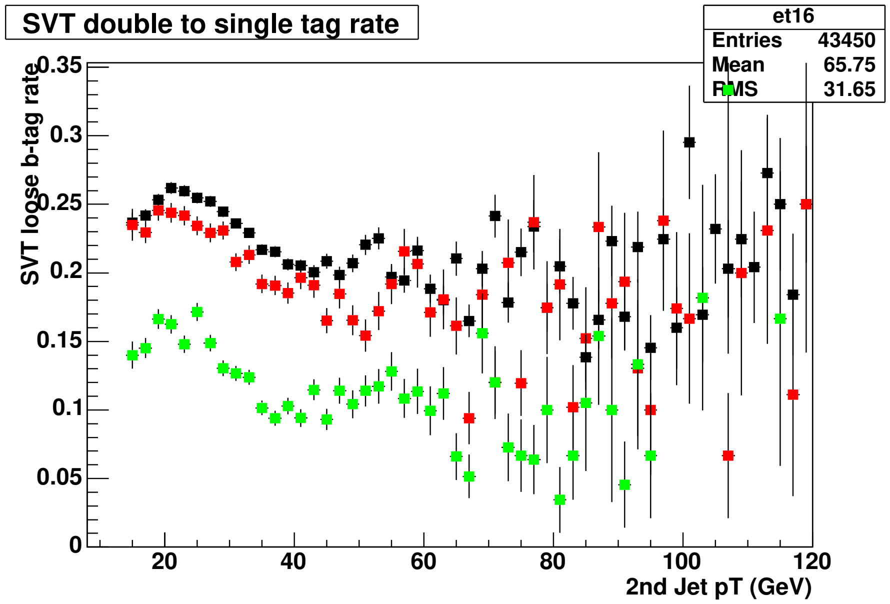

Figure 6: TRF as a function of second-leading jet p_T for jets in the regions $\mid \eta \mid < 1.1$ (black), 1.1 $< \mid \eta \mid < 1.5$ (red) and $1.5 < \mid \eta \mid < 2.5$ (green), evaluated for in-zone events in pre-v13 data.

6.4 Comparing The Background Models to Data

The described background model - with a jet-based TRF - is now applied to the entire pre-v13 data. Figure 7 shows the fit of the background prediction (from the in-zone TRF) to the double tagged data in the high mass region. The normalization correction is given by the single fit parameter "bkg".[7]

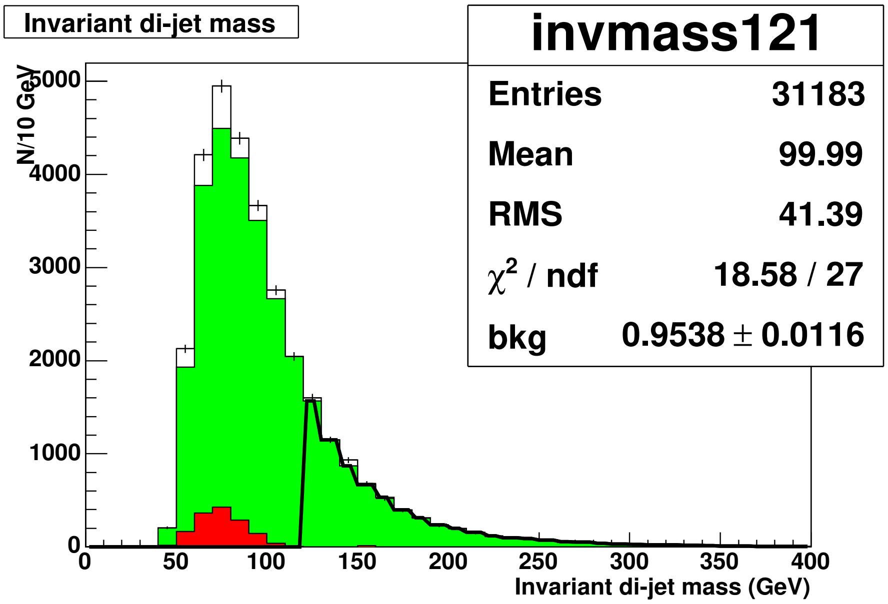

Figure 7: Invariant dijet mass in the pre-v13 data *before* background subtraction. Green (light gray) shaded histogram: expected background, estimated using a jet-based TRF from in-zone events and fit with a one parameter fit to the observed data above 120 GeV. Black points: total dijet mass distribution observed in data. Red (dark gray) histogram: expected $Z \to b\bar{b}$ signal from MC. The fit results in a correction to the background scale of 0.9538 $\pm$ 0.0116.

The normalised invariant mass background compared to data and signal MC is shown in Figure 8. Figure 9 shows the invariant mass after subtraction of the background.

A complete mass-bin-by-mass-bin breakdown of the excess in pre-v13 data and Monte Carlo is presented in Table 8. After background subtraction we observe an excess of

$$1352.8 \pm 151.33 \text{ (stat.)} \pm 305.70 \text{ (syst.) events } [\textit{pre-v13 data, 297.5 pb}^{-1}]$$

in the 50–100 GeV/c^2 mass window, as plotted in Figure 9. The excess peak is fitted with a Gaussian and compared to the number of events expected from Monte Carlo. We expect to see

$$1388.92 \pm 107.09 \text{ (stat.) events } [\textit{Signal Monte Carlo, with pre-v13 trigger}]$$

and therefore observe good agreement between data and Monte Carlo within the errors. Table 9 summarizes the overall pre-v13 excess.

[7]By construction this method produces a background invariant mass template with an identical number of integrated events as the observed double-tags. If the invariant mass shape of the background and observed data were identical then the normalization would be equal to 1. The fact that the fit yields 0.96 indicates a difference in the relative fraction of events above and below 120 GeV in the background template and the double-tagged data. We have more events in the Z mass region in the double-tagged data.

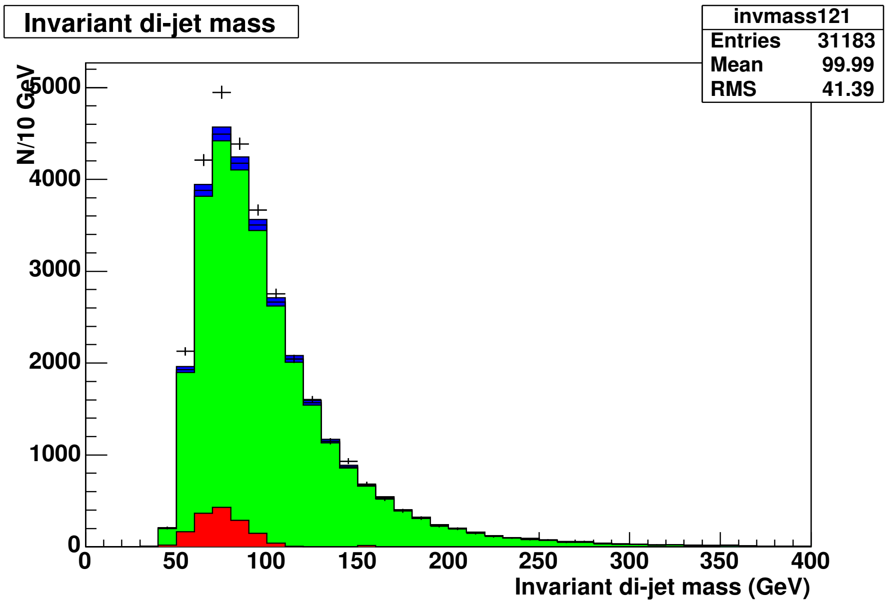

Figure 8: Invariant dijet mass in the pre-v13 data *before* background subtraction. Green (light gray) shaded histogram: expected background, estimated using a jet-based TRF from in-zone events. The dark blue band indicates the $\pm$ 1.7 % systematic error on the background. Black points: total dijet mass distribution observed in data. Red (dark grey) histogram: expected $Z \rightarrow b\bar{b}$ signal from MC.

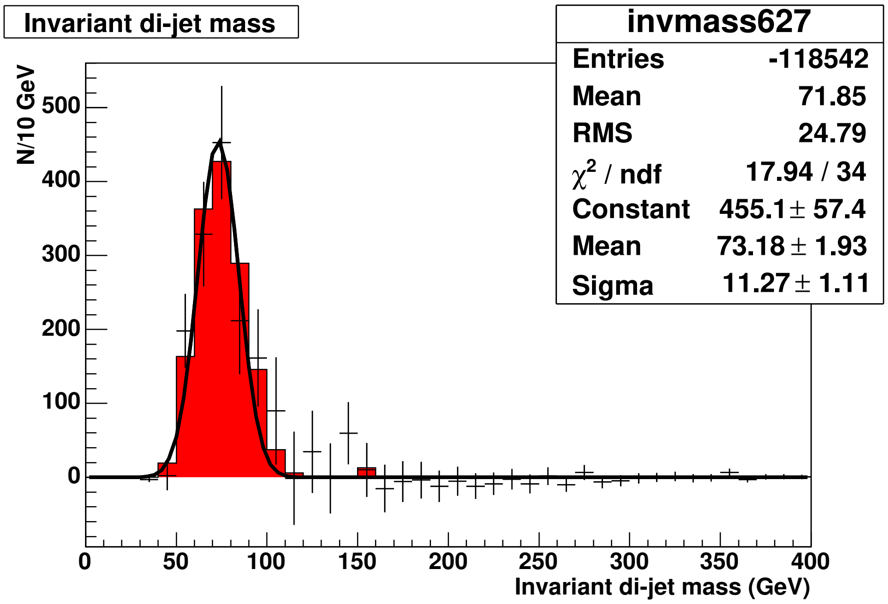

Figure 9: The invariant dijet mass spectrum in the pre-v13 data *after* background (from in-zone TRF) subtraction. Black points: excess observed in data, fitted with a Gaussian. Error bars show statistical errors only. Red (dark gray) histogram: expected signal from MC. The excess peak has a mean mass of 73.18 GeV/c^2 and a width of 11.27 GeV/c^2.

The total statistical error is calculated by combining in quadrature the statistical errors on the number of observed events and expected background events. The main source of systematic uncertainty on the observed excess comes from the normalization fit of the background and is taken, from the error on the fitted parameter, to be 1.3% of the number of background events. The contribution from the invariant mass shape of the TRF based background not being modeled perfectly, is estimated to be small from the small χ^2/NDF of the normalization fit at masses above 120 GeV. A study of the difference of the invariant mass shape of an un-tagged (light quark dominated) and single-tagged (b contaminated) event sample, similar to the 0 to 1 tag correction in Section 7, reveals a net uncertainty on the number of background events of less than 1% in the 50-100 GeV Z mass region. Hence, an additional 1% systematic uncertainty was added to the error on the background.

The systematic error on the background is added in quadrature to the total statistical error in the last column of Table 9. Taking the systematic uncertainty of the background into account, the observed excess has a significance of 4.0 standard deviations.

The peak of the distribution lies at approximately 75 GeV/c^2, in both Monte Carlo and data, after jet energy scale corrections have been applied. At the time of this analysis no official b-jet JES correction, other than the correction for muons in jets, is available for this data. Applying an unofficial b-jet JES correction to the MC shifts the peak to 79 GeV. The remaining mass shift could be explained by energy loss to hard final state radiation as suggested in [3].

Invariant Mass Bin (GeV/c^2)	**No. Events Observed**	**No. Events Expected**	**Excess**	**Expected $Z \to b\bar{b}$**
0–30	0	0	0	0
30–60	2336	2138.45 ± 20.59	197.56 ± 52.54	166.74 ± 29.21
60–90	13543	12549.70 ± 49.88	993.30 ± 126.62	1064.96 ± 73.82
90–120	8465	8215.07 ± 40.36	249.93 ± 100.47	191.41 ± 31.30
120–150	3682	3589.04 ± 26.68	92.96 ± 66.28	4.23 ± 4.65
150–180	1590	1600.98 ± 17.82	-10.98 ± 43.67	16.15 ± 9.09
180–210	731	752.03 ± 12.21	-21.03 ± 29.67	0
210–240	354	377.46 ± 8.65	-23.46 ± 20.71	0
240–270	201	218.26 ± 6.58	-17.26 ± 15.63	0
270–300	117	121.73 ± 4.91	-4.73 ± 11.88	0
300–330	67	67.51 ± 3.66	-0.51 ± 8.97	0
330–360	44	39.39 ± 2.79	4.61 ± 7.20	0
360–390	19	20.54 ± 2.02	-1.54 ± 4.80	0

Table 8: Signal candidate counts before and after background subtraction in the pre-v13 data and MC. The errors are statistical only.

Search Window ($\mathrm{GeV/c^2}$)	**No. Events Observed**	**No. Events Expected**	**Overall Excess**	**Total Stat. Error**	**Total Syst. Error**	**Overall Error**
50–100	19335	17982.20	1352.80	151.33	305.70	341.10
Prediction from MC: 1388.92 ± 107.09						
Significance of Result: 3.97 $\boldsymbol{\sigma}$						

Table 9: Excess of events observed in the 50–100 $\mathrm{GeV/c^2}$ search window after background subtraction has been performed in the pre-v13 data, along with the signal prediction from MC. Agreement is seen between the excess observed and the number of signal events predicted.

6.5 Closure Test

As a closure test, the sum of the invariant mass templates of the signal MC and background from the in-zone TRF were fitted to the whole invariant mass range of the observed double tagged candidates. The scale of the two templates were fitted with two unbound scale parameters: "bkg" and "signal" (see Figure 10).

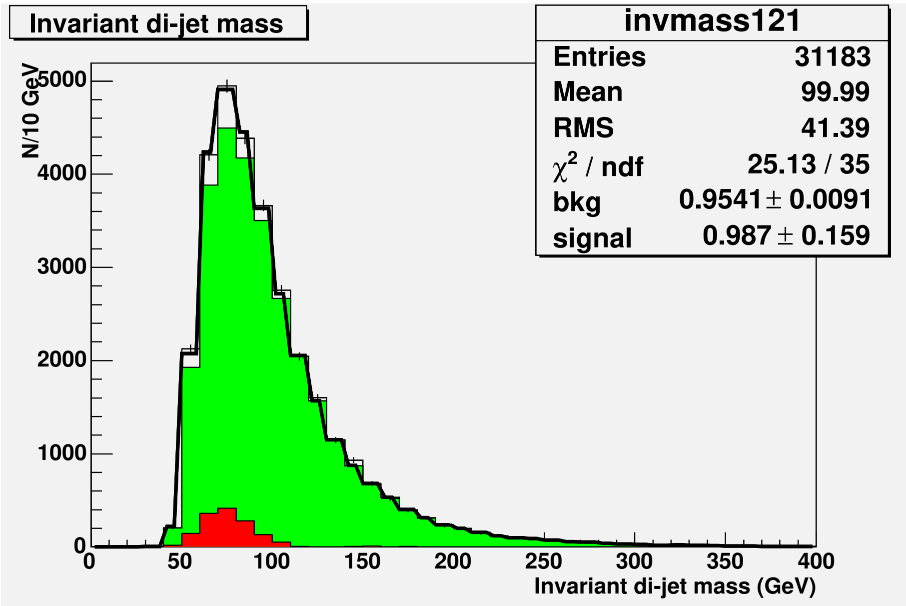

Figure 10: Closure test of the final invariant dijet mass spectrum observed in the pre-v13 data after background subtraction. Green (light gray) shaded histogram: expected background, estimated using a jet-based TRF from in-zone events. Black points: total dijet mass distribution observed in data. Red (dark gray) histogram: expected signal from MC. The bold black line shows the fitted sum of the scaled background and MC templates.

As can be seen, the fitted background scale parameter is 0.9541 ± 0.0091, which within the error is compatible with the value obtained from Figure 7. The fitted signal scale parameter is within errors compatible with the expected value 1, we therefore conclude that the sum of the signal MC and the background as calculated with our in-zone TRF based model and normalised to the high mass region, are compatible with the observed double tagged invariant mass over the full region. Furthermore, adding the signal MC to the background template is necessary in order to obtain a good fit to the data.

7 Background Estimation Method 2: The Full TRF Method with 0→1 and Z Corrections

Another method of background estimation will now be discussed; it differs from the previous method in the following ways:

- The full pass1 pre-v13 data set is used, with no trigger selection. Pass1 data did not use the T42 correction and has a different version of the jet energy scale corrections than the pass2 data.
- A slightly tighter primary vertex requirement is made, with ≥4 tracks attached, and $|z| < 35$ cm (the fiducial b-tagging region).
- The method does not assume that the signal or background is dependent on $\Delta\varphi$. The jet-based TRF is measured in, and applied to, the same data sample, as was done in the "in-zone TRF" method discussed above.
- A slightly wider $\Delta\varphi$ cut was used, > 2.9 instead of > 3.0.

In addition, two corrections are applied to this background estimation:

- Because the TRF is applied to the single-tagged data sample, which is less rich in heavy-flavour jets than the data sample to which it is compared (the double b-tagged data), any differences in either the jet-energy-scale of heavy-flavour jets as opposed to gluon and light-quark jets or their natural invariant mass spectrum will result in a shift of the invariant mass distribution expected for the background, as compared to the data. The shift is observed and measured using an *untagged* data sample. A TRF is derived for the un-tagged data and applied to the untagged data, and then compared to the actual single-tagged data. The shift which is derived is called the "0→1" correction, which is then subtracted from the expected background in the double-tagged data sample. This correction relies on the fact that each successive b-tag that is required increases the fraction of heavy-flavour by the same amount. This is verified by comparing the data with MC $b\bar{b}$ events.
- The effects of $Z \to b\bar{b}$ events which are present in both the un-tagged and single-tagged data samples from which the 0→1 correction and the TRF are derived, respectively, are corrected for. A signal peak is first measured in double-tagged data, using this background subtraction method, including the 0→1 correction. The number of events which would exist from this signal peak in the un-tagged and single-tagged data samples is then extrapolated using a $Z \to b\bar{b}$ MC sample with no, one, and two b-tags required. The signal peak, *measured in data*, is then scaled by these factors and subtracted from the un-tagged and single-tagged samples. Then the TRF and the 0→1 correction are re-derived, the expected background in the double-tagged data is re-calculated, and a new signal peak is observed. This correction process is then repeated, using the new signal peak to estimate the $Z \to b\bar{b}$ events in the un-tagged and single-tagged data samples, a total of three times, after which the correction and signal peak are stable.

7.1 The $0 \to 1$ tag Shift

As described above, the shift in the invariant mass spectrum of the dijet system caused by applying a single b-tag is first measured. Later this will be subtracted from the estimated background of the double b-tagged data. A TRF is derived on the un-tagged sample (see Figure 11) and re-applied to the same un-tagged data sample, to predict the background to the single-tagged data sample, as shown in Figure 12. A comparison is also shown in this figure to the $b\bar{b}$ MC dijet invariant mass spectrum (which was normalized using double-tagged data). The $b\bar{b}$ events make up about 10% of the single-tagged data sample, as opposed to about 2% in the un-tagged data sample. The small contribution of $Z \to b\bar{b}$ expected in the single-tagged data is also shown. Most of the events in the single-tagged data sample contain only gluon/light-quark jets.

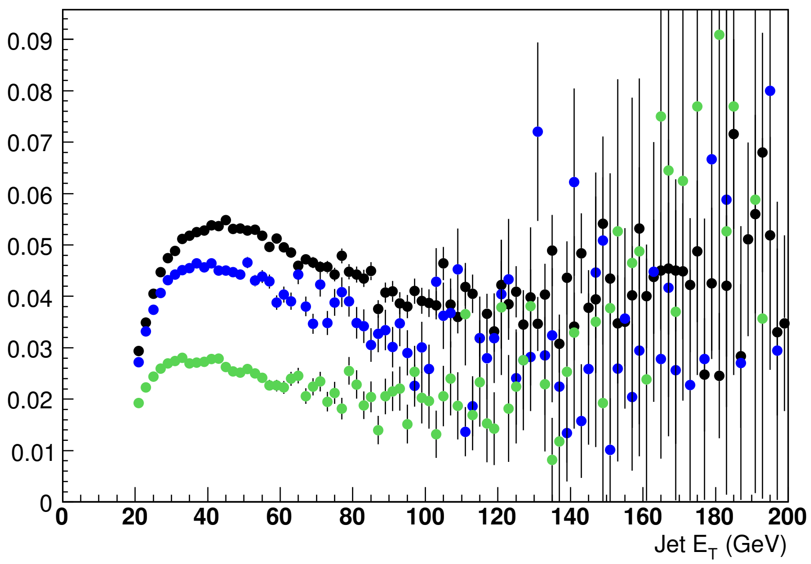

Figure 11: The TRF's derived on the un-tagged data sample, which are used to estimate the single-tagged background. Each TRF is a function of corrected jet p_T in one of three η-bins: $\eta < 1.1$, $1.1 < \eta < 1.5$, and $1.5 < \eta < 2.5$.

The difference between the single-tagged data and the expected background from the TRF is shown in Figure 13. A comparison of the background-subtracted single-tagged data to the MC $Z \to b\bar{b}$ invariant mass distribution shows that it is not the result of a signal peak in the single-tagged data, but rather an overall shift in the invariant mass distribution. As mentioned above, this shift is understood to come from either a difference between the gluon/light-quark and the b-quark jet energy scale factors or a difference in the ratio of true cross-section of heavy-flavour jets to light-jets as a function of dijet invariant mass.

7.2 The Double-tag TRF

To estimate the double b-tagged background, a set of TRFs are derived as a function of corrected jet p_T for 3 η-bins from the single-tagged data and reapplied to the same data. The TRFs are shown in Figure 14. The resulting estimate of the double-tagged background is compared to double-tagged data and shown in Figure 15.

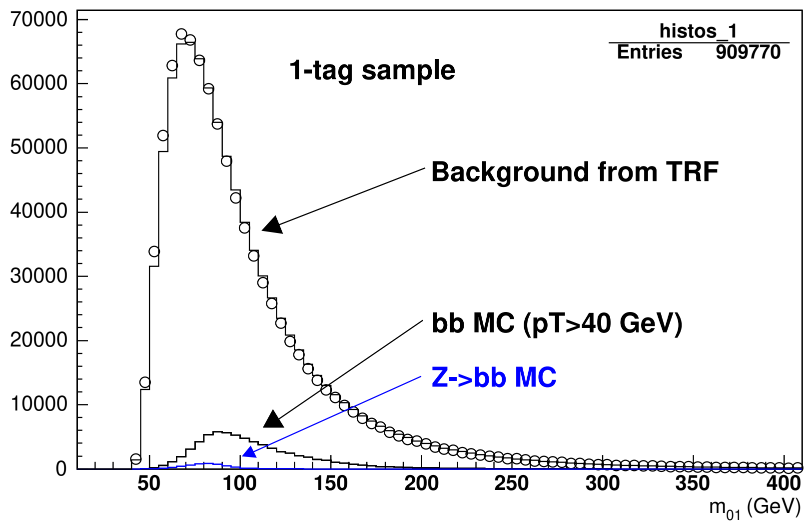

Figure 12: Comparison between the single-tagged data and the background expected using the TRF method. Comparisons are also shown to the $b\bar{b}$ MC dijet invariant mass spectrum (which was normalized using double-tagged data) and to the $Z \to b\bar{b}$ MC dijet invariant mass spectrum, to give a feel for the composition of the sample. The rest of the events are thought to be gluon/light-quark jet events.

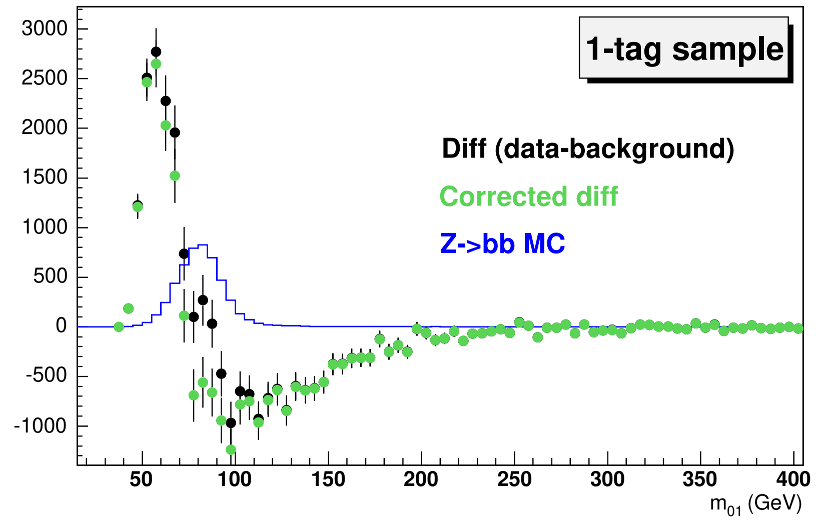

Figure 13: Difference between the single-tagged data and the background expected using the TRF method, a measure of the 0→1 tag shift, which will be subtracted from the expected double b-tagged data (after proper normalization). The difference is also shown after correcting for the expected $Z \to b\bar{b}$ events in the un-tagged and single-tagged data samples, using the methods described below in Section 7.3.

7.3 The 0- and 1-tag Z Peak Correction

As mentioned above, the un-tagged and single-tagged data samples contain signal events, which will now be corrected for. The signal peak observed in double-tagged data, after subtracting the

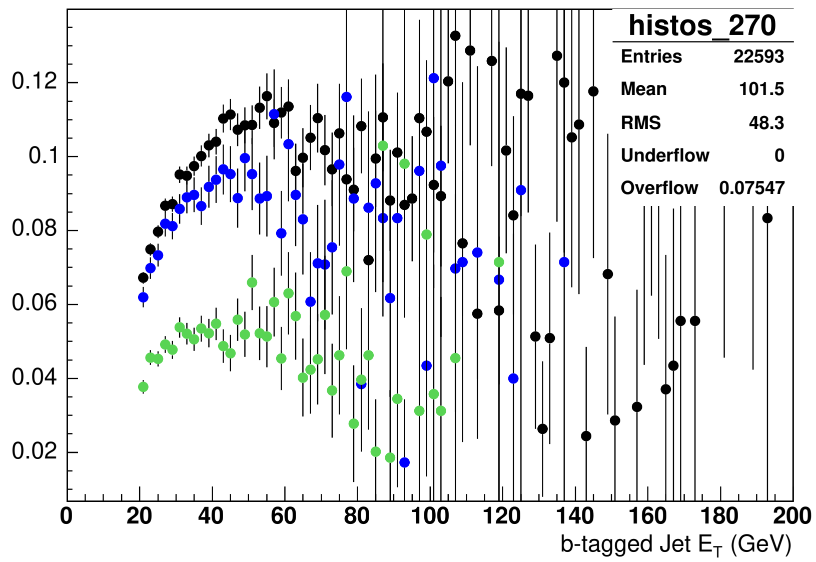

Figure 14: The TRF's derived on the single-tagged data sample, which are used to estimate the double-tagged background. Each TRF is a function of corrected jet p_T in one of three η-bins: $\eta < 1.1$, $1.1 < \eta < 1.5$, and $1.5 < \eta < 2.5$.

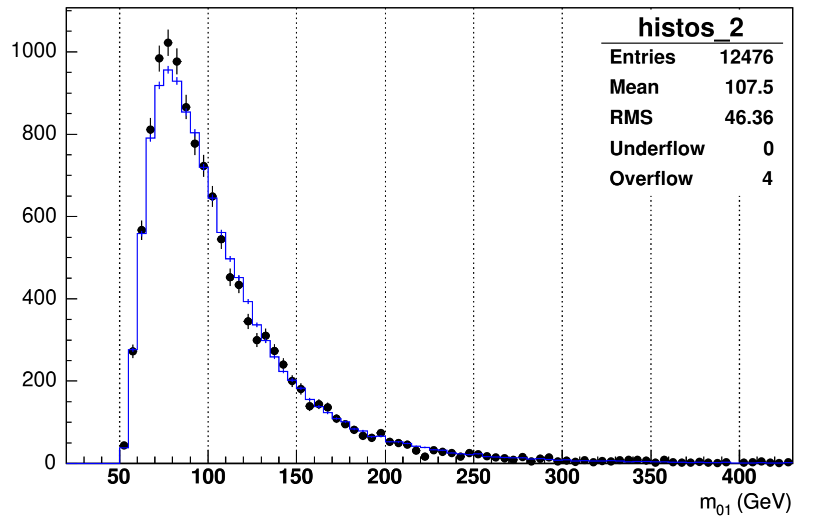

Figure 15: The comparison between double b-tagged data (points) and the expected background, from the TRF method using single-tagged data, before either of the background corrections ($0 \rightarrow 1$ or Z peak).

estimated background using the TRF method, is scaled by a factor of 6.5, which is the ratio of single-tagged to double-tagged events in the $Z \rightarrow b\bar{b}$ MC sample. It is important to note that the MC is only used for an overall normalization (the b-tagging efficiency), and does not affect the shape of the signal peak. This scaled signal peak is then divided (bin by bin) by the single-tag data, to determine the estimated fraction of $Z \rightarrow b\bar{b}$ events in each bin of the single-tag data, as shown in Figure 16.

The expected fraction of $Z \to b\bar{b}$ events in each invariant mass bin is then subtracted from the signal-tagged data (the events are weighted by 1-f, where f is the fraction of $Z \to b\bar{b}$ expected). Then the TRFs are re-derived and re-applied to this corrected, weighted, single-tagged data. The 0→1 tag correction is also re-derived, using the same principles to estimate the fraction of $Z \to b\bar{b}$ in the un-tagged data sample. The effect from $Z \to b\bar{b}$ events in the un-tagged sample is relatively small, as expected, so the modification to the 0→1 tag correction is slight, as seen in Figure 13.

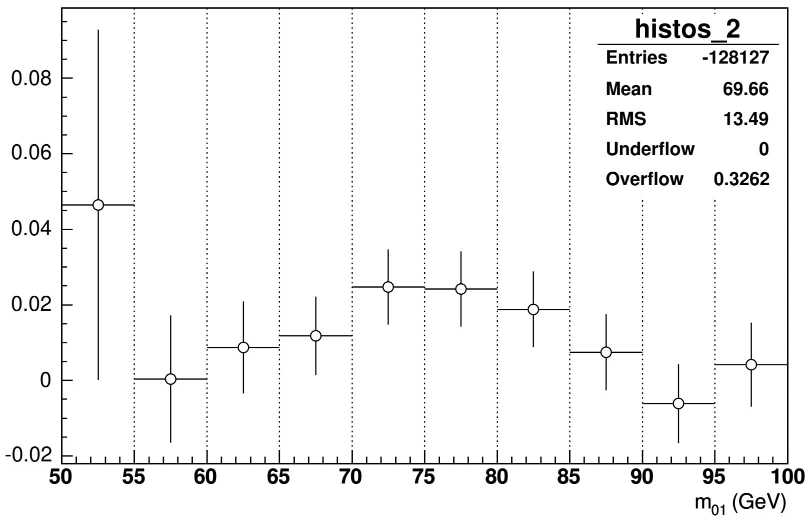

Figure 16: The estimated fraction of $Z \to b\bar{b}$ events in the single-tagged data sample, as estimated from the peak observed in the double-tagged data sample after subtracting the background estimated via the TRF method. This fraction of events will be subtracted from the single-tagged data, and then the final TRFs are derived and re-applied to this corrected single-tagged data set.

Since the size and shape of the original Z peak in data changes slightly after the corrections to the un-tagged and single-tagged data, the corrections themselves can be re-derived using the new Z peak observed. This cyclic process could be continued ad-infinitum, but in practice the solution is stable after only a few iterations, which results in a final Z peak and set of corrections.

7.4 Applying This Full-TRF Method to Data

After Z peak corrections to the un-tagged and single-tagged data samples, the comparison of the background-subtracted double-tagged data to the observed 0→1 tag shift is shown in Figure 17. (The slightly different shape of the 0→1 tag shift without Z peak corrections to the un-tagged and single-tagged data samples is also shown, to give a feel for the size of the effect.)

The final $Z \to b\bar{b}$ peak derived from data, after all corrections, is considered to be the difference between the background-subtracted double-tagged data and the corrected 0→1 tag shift. This invariant mass distribution difference is shown in Figure 18, and compared to the shape of the $Z \to b\bar{b}$ distribution in MC. (The slightly different shape of the difference between the background-subtracted double-tagged data and the 0→1 tag shift without Z peak corrections to the un-tagged and single-tagged data samples is also shown, to give a feel for the size of the effect.)

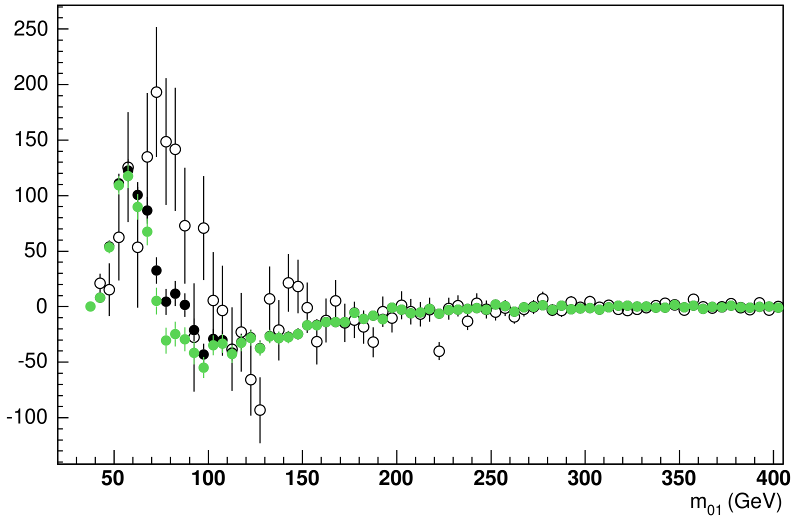

Figure 17: Comparison of the background-subtracted double-tagged data (white squares) to the observed 0→1 tag shift (green). The slightly different shape of the 0→1 tag shift without Z peak corrections to the un-tagged and single-tagged data samples is also shown (black), to give a feel for the size of the effect.

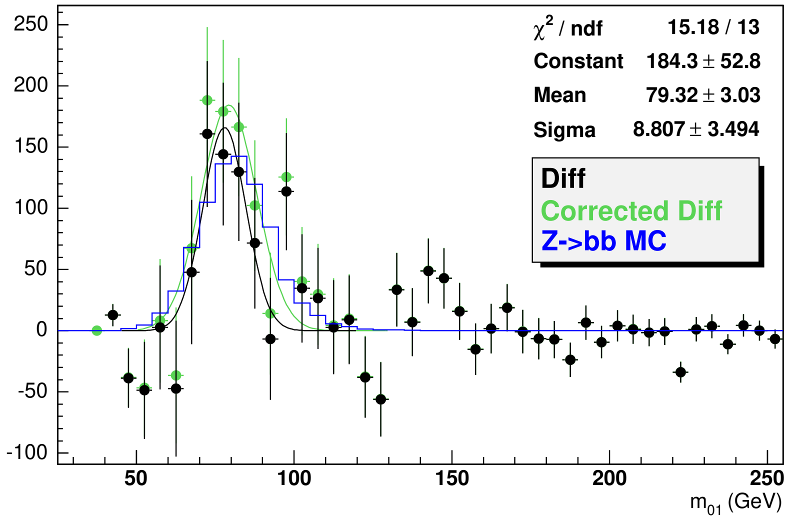

Figure 18: The final $Z \to b\bar{b}$ peak derived from data, after all corrections (green), compared to the shape of the $Z \to b\bar{b}$ distribution in MC (blue). (The slightly different shape of the Z peak in data without the Z peak corrections to the un-tagged and single-tagged data samples (black) is also shown, to give a feel for the size of the effect.)

The final Z peak in data (with all corrections included) is fit to a Gaussian distribution, which describes the shape of the $Z \to b\bar{b}$ peak well in MC. Both the mean (79±3 GeV) and width (9±3 GeV) of the distribution observed for data are comparable to those derived from $Z \to b\bar{b}$ MC: 81 GeV and 11 GeV, respectively.

810±230 $Z \rightarrow b\bar{b}$ events are observed, where the error is taken from the uncertainty in the height of the Gaussian fit. Recall that the data set used to test this background estimation method is able to use a larger $\Delta\varphi$ range (2.9 as opposed to 3.0), spans the pre-v13 trigger-list data in the Pass1 skim, and corrects for the signal events in the data from which the TRFs were derived. (570±160 events are observed if the signal events in the data from which the TRFs were derived are not corrected for.) The total number of events expected from $Z \rightarrow b\bar{b}$ MC can not be estimated very accurately, because the data were not selected by a given trigger. However, for an assumed luminosity of 300 pb^{-}1, the size of the $Z \rightarrow b\bar{b}$ peak observed in data would correspond to an overall trigger/skimming efficiency of about 15% (note that this agrees with the efficiencies presented in Section 3). This efficiency is reasonable since the trigger/skimming require a muon, and the signal has two b-jets, each with a 10% branching ratio to muons.

8 Summary of Results

We have investigated different methods to extract an observable $Z \rightarrow b\bar{b}$ signal in the p14 data from the BID skim. Using a jet based TRF from events in the back to back $\Delta\varphi$ region to model the background we observe the following excess in 297.5 pb^{-1} of data collected with the MU_JT25_L2M0 trigger:

$$1352.80 \pm 151.33 \text{ (stat.)} \pm 305.70 \text{ (syst.)}$$

compared to MC expectations of:

$$1388.92 \pm 107.09 \text{ (stat.)}$$

The observed signal amounts to a significance of 4.0 standard deviations.

A second approach, without trigger selection, but correcting for the Z contribution to the TRF, also confirms the observed excess:

$$810 \pm 230 \text{ (stat.)}$$

The position and width of the observed mass peak are in both cases in agreement with MC expectations. Method 1 finds a peak with a fitted mean of 73±2 GeV and method 2 a fitted mean of 79±3 GeV. The difference between the observed mass peaks can be attributed to the different data samples and JES corrections (p14 pass2 versus pass1) and to the different event selection applied. MC studies have shown that the reconstructed peak position is sensitive to both trigger as well as muon and jet p_T requirements.

Worth noting is also the interesting small excess around di-jet masses of 140 GeV, which is seen in the data with both methods.

9 Conclusions

We have demonstrated that a $Z \rightarrow b\bar{b}$ di-jet mass resonance indeed successfully can be isolated from the massive QCD background, already with the first 300 pb^{-1} of RunII data collected by the DØ experiment. The observed excess agrees well with the expectations from $Z \rightarrow b\bar{b}$ MC.
Thanks to the new dedicated $Z \rightarrow b\bar{b}$ triggers we have already collected a several times larger data sample which is now waiting to be analyzed. The larger statistics from this sample is not only expected to provide a larger Z peak but also enable a more precise background determination.

References

[1] T. Dorigo,*Observation of Z Decays to b Quark Pairs at the Tevatron Collider*, hep-ex/9806022.

[2] A. Haas *et.al.*,*DØSearch for Neutral Higgs Bosons at High tanβ in Multi-jet Events Using p14 Data*, DØ note 4671.

[3] A. Jenkins and A. Goussiou, *An Investigation of b-jet Energy Resolution in $Z^0H^0 \rightarrow eeb\bar{b}$ and* $Z^0 \rightarrow b\bar{b}$, DØ Note 4136.

Appendix A: Trigger list v13

A set of five dedicated $Z \to b\bar{b}$ triggers were designed to run unprescaled up to luminosities of about 80 x 10^{30} $\text{cm}^{-2}\text{s}^{-1}$ as part of the v13 trigger list. Table 10 provides a description of these new trigger terms. Three of the triggers identify single-muon events using either b-tagging or muon selection at Level 3. The other two triggers select clean but rare dimuon events. The aim was to construct a versatile set of triggers which cover different characteristics of the $Z \to b\bar{b}$ decay.

v13 Trigger	**Trigger Description**		
	Level 1	**Level 2**	**Level 3**
ZBB_TLM3_2JBID_V	single μ + track	$\geq 1\mu$	$\geq 1\mu$, IP tag, vtx cut, 2 jets
ZBB_TLM3_2LM0_2J	single μ + track	$\geq 1\mu$	≥ 2 medium μ, 2 jets
MUJ1_2JT12_LMB_V	single μ + 2 jets	$\geq 1\mu + \geq 1$ jet	IP tag, vtx cut, μ, $\geq$2 jets
MUJ2_2JT12_LMB_V	single μ + jet	$\geq 1\mu$	IP tag, vtx cut, μ, $\geq$2 jets
DMU1_JT12_TLM3	dimuon term	$\geq 1\mu$	$\geq$1 trk-matched μ, jet

Table 10: Description of the new v13 $Z \to b\bar{b}$ triggers. "trk-matched" means track-matched; "vtx cut" means vertex cut.

The v13 data exploited in this study were collected between early June 2004 and the end of August 2004, when the Tevatron shutdown commenced. Each v13 trigger was exposed to approximately 50–60 pb^{-1} of integrated luminosity, which reduces to about 50 pb^{-1} after good run selection (see Table 11).

v13 Trigger	**Luminosity (pb^{-1})**		
	Delivered	**Recorded**	**Good**
ZBB_TLM3_2JBID_V	68.9	49.7	45.9
ZBB_TLM3_2LM0_2J	68.9	49.7	45.9
MUJ1_2JT12_LMB_V	68.9	53.8	48.9
MUJ2_2JT12_LMB_V	68.9	51.6	47.4
DMU1_JT12_TLM3	68.9	62.0	54.2

Table 11: Delivered, recorded and good luminosity for the v13 $Z \to b\bar{b}$ triggers. This analysis incorporates only good luminosity data. The dimuon trigger was exposed to a larger integrated luminosity as it remained unprescaled. The single-muon triggers were prescaled or turned off at the very highest luminosities.

The trigger rates and signal candidate yield of the most significant v13 triggers are described in Table 12.

Table 13 lists the trigger efficiencies for the v13 triggers, evaluated by passing signal Monte Carlo events through a full trigger simulation (`d0trigsim`). Trigger efficiencies are quoted for each trigger individually and in combination (as an ORed term). The fraction of events passing all three trigger levels is calculated with respect to both absolute number of events and events passing offline cuts.

The v12 and v11 triggers are slightly more efficient than the v13 triggers as a result of looser L3 conditions (in particular no IP-tag or primary vertex requirements). The tighter v13 conditions are needed to avoid prescales at instantaneous luminosities above 50E30. The events from the v13 data

v13 Trigger	Trigger rate at L=60E30	Signal candidate yield
MUJ1_2JT12_LMB_V	1.24 Hz	3741
MUJ2_2JT12_LMB_V	1.09 Hz	3349
MM1_JT25	2.09 Hz	2874
ZBB_TLM3_2JBID_V	0.95 Hz	2727

Table 12: The trigger rates and signal candidate yields, in the v13 portion of the data, for the four leading v13 $Z \to b\bar{b}$ triggers. Note that all of the three single muon based specifically designed $Z \to b\bar{b}$ triggers from Table 3 are among the four leading triggers and that MM1_JT25, which is a B-phyics trigger, has a higher rate.

v13 Trigger	L1L2L3 Trigger Efficiency(%)	
	Absolute	w.r.t. Offline Cuts
MUJ1_2JT12_LMB_V	3.3	11.1
MM1_JT25	3.8	11.8
MUJ2_2JT12_LMB_V	3.3	11.6
ZBB_TLM3_2JBID_V	2.7	9.3
OR of the above 4 triggers	6.0	16.9

Table 13: v13 trigger efficiencies for MC signal events.

were selected exclusively from the MUJ1_2JT12_LMB_V trigger which was exposed to a luminosity of 48.9 pb^{-1}. Tables 14 and 15 show the number of events passing each analysis cut in signal MC and data. Monte Carlo event counts are weighted by cross-section and luminosity.

Analysis Cut	Number of Events Passing Cut, v13
No selection	55204 ±193
1 (MUJ1_2JT12_LMB_V)	1814 ± 36
2	1012 ± 26
3	783.7 ± 23
4	745.8 ± 22
5	716.0 ± 22
6	183.3 ± 11
7($\Delta\phi > 3.0$)	120.4 ± 10

Table 14: Cut flow table for $Z \to b\bar{b}$ Monte Carlo events passing v13 triggers. Event counts are weighted by cross-section and luminosity, the errors are statistical only.

The small v13 sample has much lower statistics than the pre-v13 data and also new triggers with different systematics, which at this time makes it difficult to extract a $Z \to b\bar{b}$ signal of any significance in this data[8].

[8] In the near future (the 1 fb^{-1} p17 analysis) it will be possible to take full advantage of the several times larger data sample which now has been collected with the new v13 and v14 $Z \to b\bar{b}$ triggers, and to exploit the potential of a significantly larger signal.

Analysis Cut	Number of Events Passing Cut, v13
1 (MUJ1_2JT12_LMB_V)	536170
2	259653
3	218002
4	179654
5	177472
6	7409
$7(\Delta\phi > 3.0)$	3741

Table 15: Cut flow table for events in data. Note the much higher fraction of events passing the offline criteria in the v13 data.

Appendix B: Estimating the background from the out-of-zone ($\Delta\varphi <$ 3.0) TRF

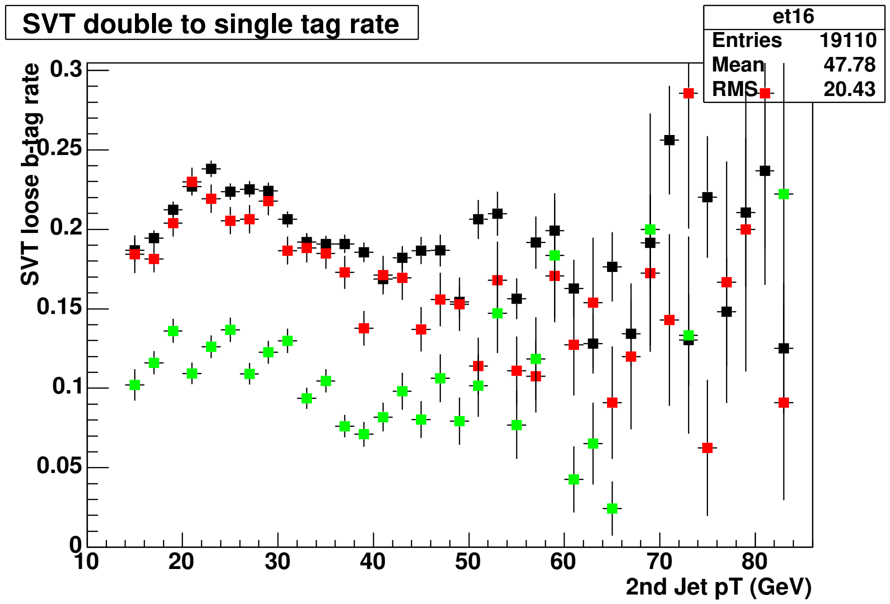

Figure 19: TRF as a function of second-leading jet p_T for jets in the regions $|\eta| < 1.1$ (black), 1.1 $< |\eta| < 1.5$ (red) and $1.5 < |\eta| < 2.5$ (green), evaluated for out of zone events in pre-v13 data.

As can be seen from plots 22 and 9, the agreement between data and signal MC is better in the case where the background was modeled with a TRF from in-zone events. The out-of-zone TRF results in a 4 GeV lower mass peak indicating that there indeed is a $\Delta\varphi$ dependent invariant mass bias. In combination with the larger statistics for the TRF determination, better data agreement at high masses and the smaller normalization correction for the in-zone TRF case, seen in Figure 7, we conclude that this method gives the most accurate result and is hence used to extract the following results. The effect of applying the out-of-zone TRF indicates that the $\Delta\varphi$ dependence is small in terms of the observed excess, but gives shifts the observed mass.

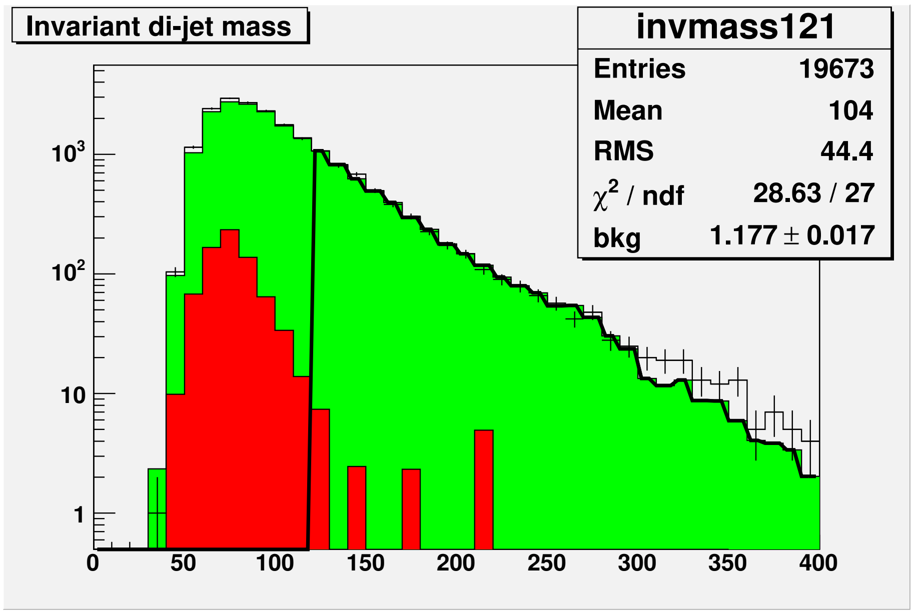

Figure 20: Invariant dijet mass in the pre-v13 data *before* background subtraction. Green (light gray) shaded histogram: expected background, estimated using a jet-based TRF from out-of-zone ($\Delta\varphi < 3.0$) events and fit with a one parameter fit to the observed data above 120 GeV. Black points: total dijet mass distribution observed in data. Red (dark gray) histogram: expected $Z \to b\bar{b}$ signal from MC. The fit results in a correction to the background scale of 1.177 ± 0.017.

Appendix C: Some additional studies from Method 2

The candidate events passing all cuts and double b-tagged in the mass range 50–100 GeV were compared between Method 1 and Method 2. As long as similar JES corrections were applied, the invariant mass reconstructed in the two analyses was very similar, as expected. Shown in Figure 23 is a comparison of the mass from Method 1 - the mass from Method 2, after just standard JES corrections.

Also investigated was the efficiency and overlap between the two analyses. Of the approximately 11,000 candidate events from Method 1:

- 739 are in bad luminosity blocks as determined from the DQ criteria for pass 1
- 1952 had the second-leading pT jet below Method 2's threshold of 15 GeV (uncorrected). Recall that Method 1 applies jet pT cuts after JES corrections.
- 5707 were not double-tagged by Method 2 (of these, 1409 had no b-tagged jets, and 4298 had one b-tagged jet)
- 21 had a poor PV (¡4 tracks)
- 99 fell outside the 50-100 M_{bb} range for Method 2
- 3101 pass all selections for Method 2

We feel that all these losses are sensible between the two analyses. Perhaps the only slightly suprising number is b-tagging. However, b-tagging did change significantly between PASS1 and PASS2, with different reconstruction and selection criteria.

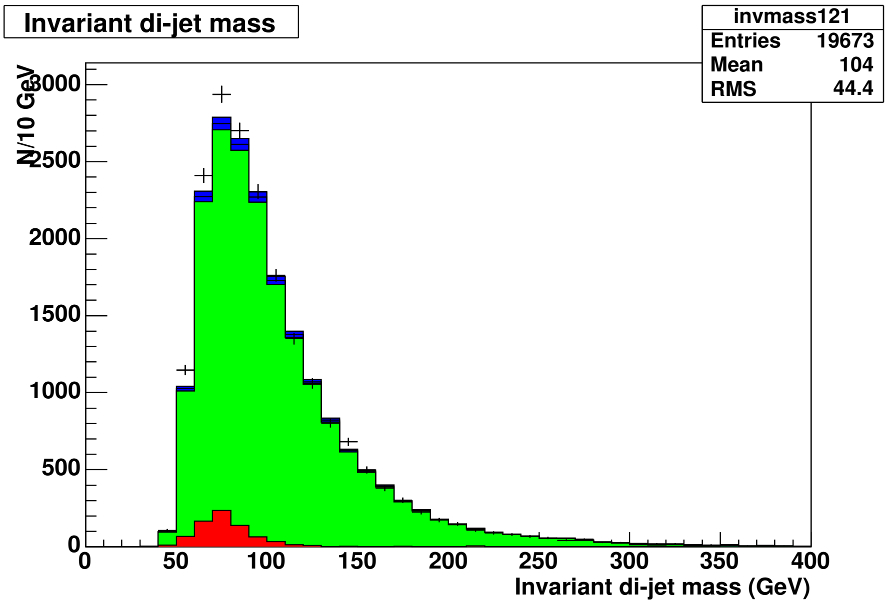

Figure 21: Invariant dijet mass in the pre-v13 data *before* background subtraction. Green (light gray) shaded histogram: expected background, estimated using a jet-based TRF from out-of-zone ($\Delta\varphi < 3.0$) events. The dark blue band indicates the $\pm$ 1.5 % systematic error from the normalisation fit. Black points: total dijet mass distribution observed in data. Red (dark grey) histogram: expected $Z \to b\bar{b}$ signal from MC.

Figure 24 shows the TRF derived from the un-tagged data sample.

The cross-section for W→cs is approximately 16 times greater than Z→bb, after including the larger W cross-section and larger BR. However, the tag rate for W→cs should be about 8 times lower than for Z→bb due to the 1/4 tag-rate for c- compared to b-jets and the fact that there's very little tag rate for the s-jet. However, this still leaves twice the contamination from W→cs as Z→bb in the single-tagged data sample. This was previously ignored in the analysis, but can be corrected for in a manner similar to the Z→bb correction in the un-tagged and single-tagged samples for TRF's. To simulate the W→cs contribution, the Z peak used for the Z-correction was tripled in size. (This makes the approximation that the peaks of W and Z have the same mass and width, compared to the resoultions available to the analysis.) Figure 25 shows the final Z-peak after making this increased correction. The peak is not significantly affected. We also note that the trigger efficiency should be lower for W→cs, since the BR to muons is lower than for bb events, so the true corrections would be even less significant. We also mention that W→cs can be safely ignored in the final double-tagged data sample, to a good approximation. W→cs will be fully simulated and included at all steps in a future incarnation of this analysis.

Several additional tests were performed, varying the analysis cuts and checking that the final Z-peak extracted from data agreed with expectations from MC in terms of size, position, and width, as shown in Figures 26 - 30. The extracted peak always agreed well with expectations from MC, giving us confidence that the peak truly is from Z→ $b\bar{b}$ production. After the $\Delta\phi$ cut was reversed to < 2.9, the peak largely disappears, as expected. When the muon-JES corrections were removed, the peak became wider, as expected, since the resolution of the jets is poorer without the correction. The peak is also of course shifted down in mass, since the corrections increase the observed jet energy. The $|\eta|$ cuts were restricted to the central (< 1.0) region and the forward

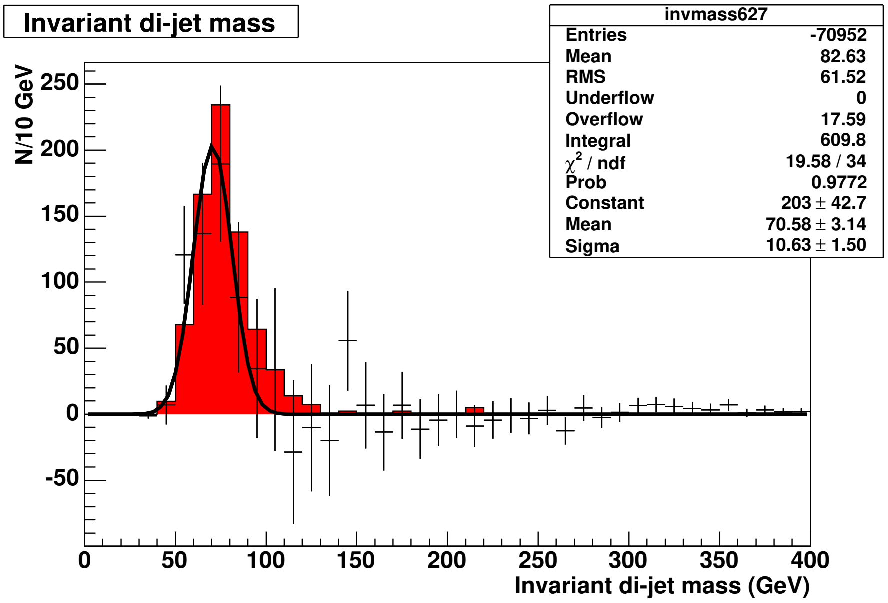

Figure 22: The invariant dijet mass spectrum in the pre-v13 data *after* background (from out-of-zone, $\Delta\varphi < 3.0$, TRF) subtraction. Black points: excess observed in data, fitted with a Gaussian. Error bars show statistical errors only. Red (dark gray) histogram: expected $Z \to b\bar{b}$ signal from MC. The excess peak has a mean mass of 70.6 GeV/c^2 and a width of 10.7 GeV/c^2.

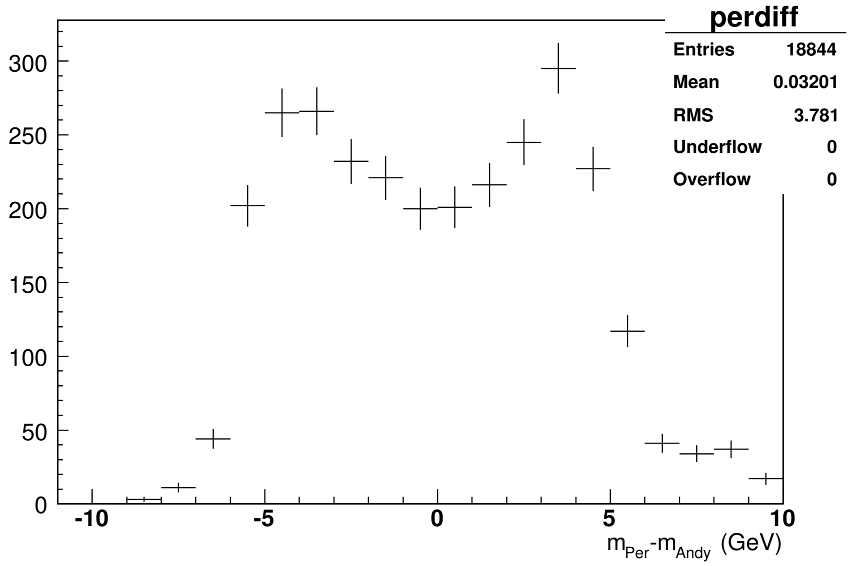

Figure 23: A comparison of the reconstructed di-jet invariant mass between candidate events in Method 1 and 2. (Mass in method 1 - Mass in method 2)

($>$ 1.0) region, and in both cases the observed number of events behaved as expected, although statistics are poor in both cases. In addition, the Z-peak corrections were not recalculated for any

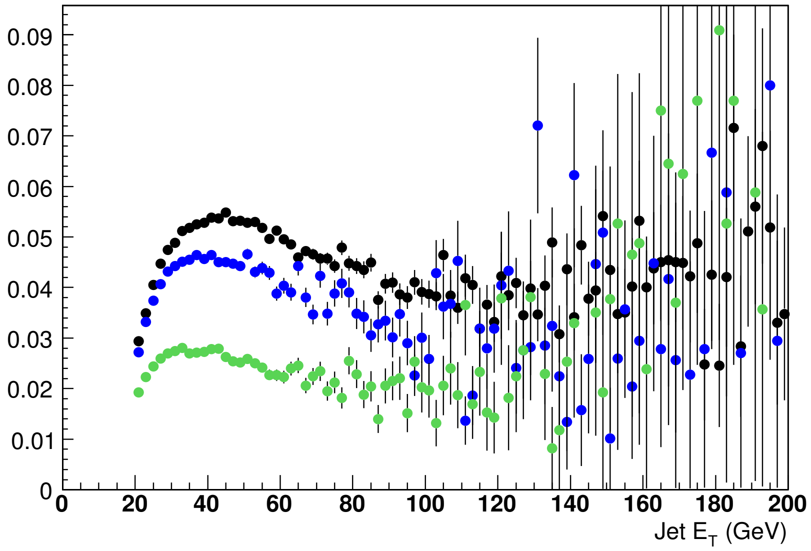

Figure 24: The TRF as measured in the untagged data sample, used for measuring the 0→1 tag shift.

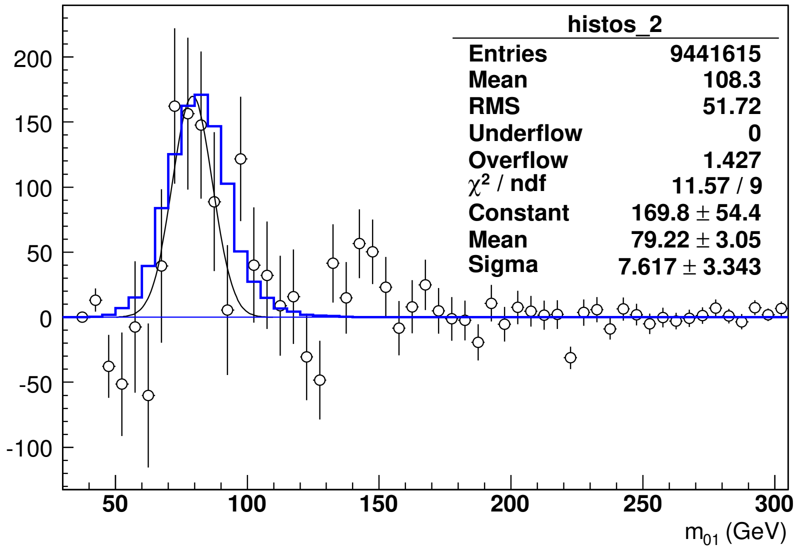

Figure 25: The final Z-peak after correcting approximately for the W→cs contribution to the single-tagged data sample.

of these cases, thus the shape of the background is slightly incorrect. The lack of the right Z-peak corrections explains the systematic excess or deficit of events in the region just above the Z-peak. Finally, the $\Delta\phi$ cut was loosened to > 2.5 (it was > 2.9), and more candidate events were observed, as expected.

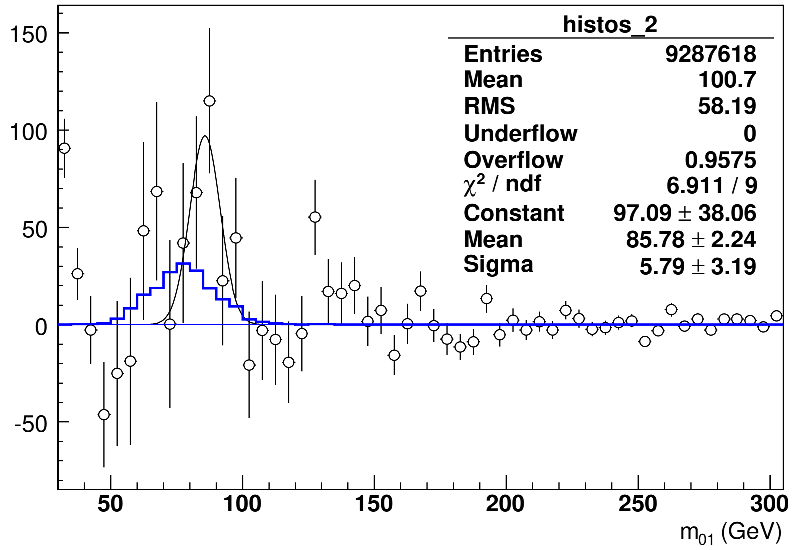

Figure 26: The final Z-peak after reversing the $\Delta\phi$ cut to <2.9.

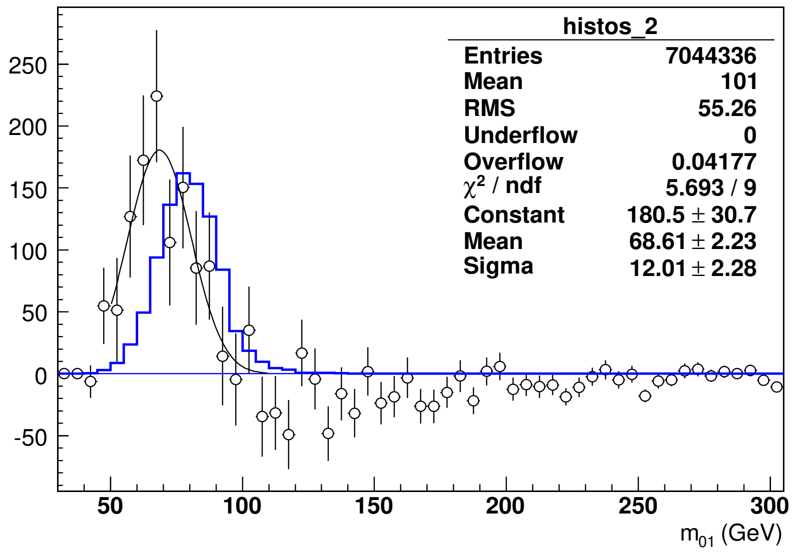

Figure 27: The final Z-peak after removing the muon-JES corrections – only the standard JES was used.

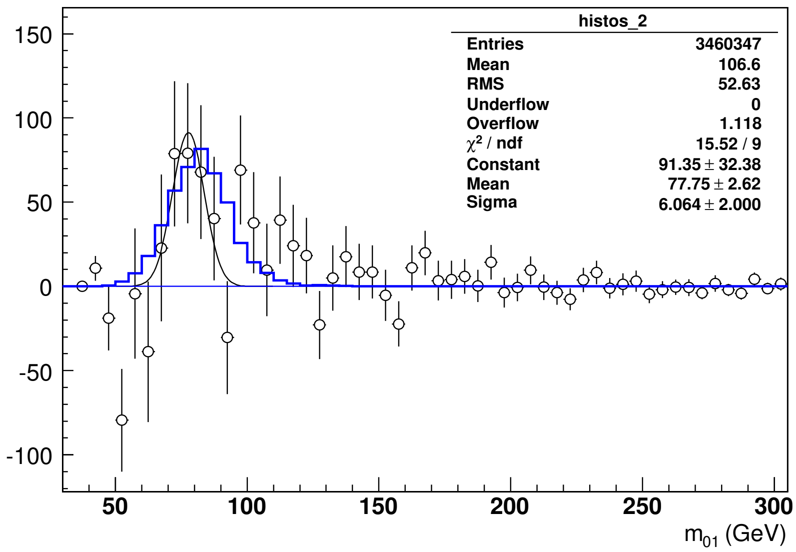

Figure 28: The final Z-peak after restricting the jet $|\eta| < 1.0$.

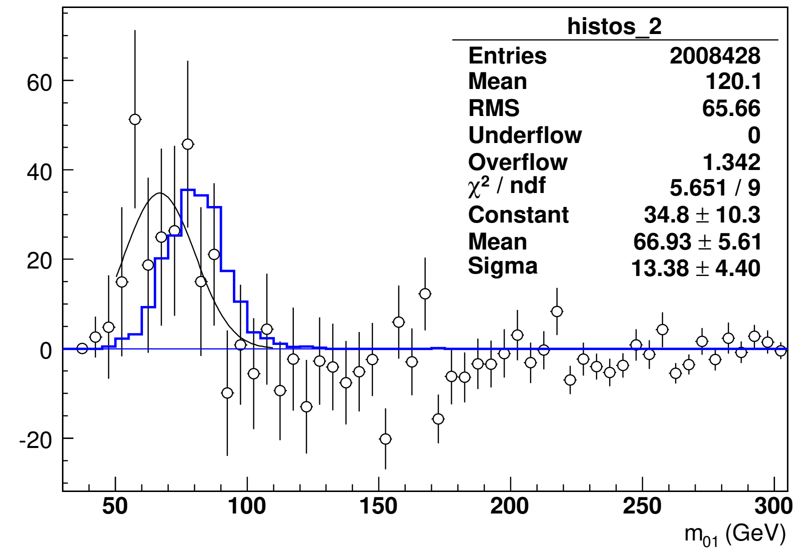

Figure 29: The final Z-peak after restricting the jet $|\eta| > 1.0$.

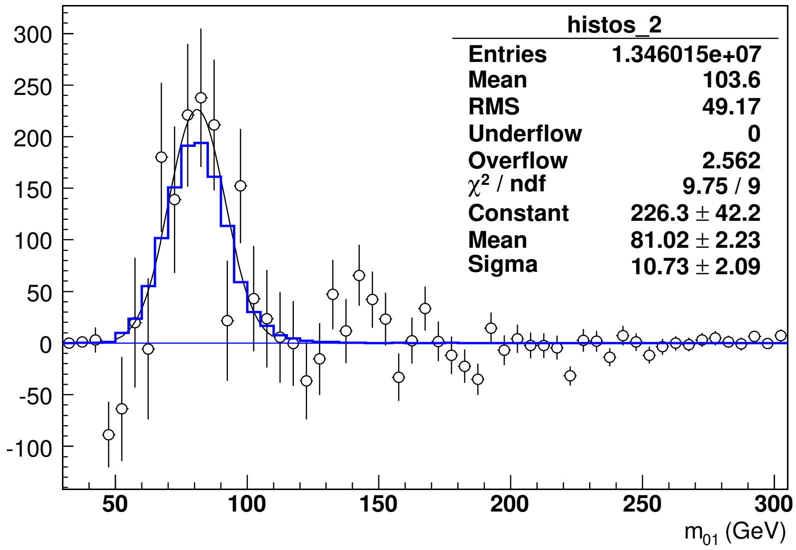

Figure 30: The final Z-peak after relaxing the $\Delta\phi$ cut to >2.5.